Published in final edited form as:
Insect Biochem Mol Biol. 2013 March ; 43(3): 260–271. doi:10.1016/j.ibmb.2012.12.005.

Biochemical properties, expression profiles, and tissue localization of orthologous acetylcholinesterase-2 in the mosquito, *Anopheles gambiae*

Picheng Zhao, **Yang Wang**, and **Haobo Jiang**
Department of Entomology and Plant Pathology, Oklahoma State University, Stillwater, OK 74078, USA

Abstract

Acetylcholinesterases (AChEs) catalyze the hydrolysis of acetylcholine, a neurotransmitter for cholinergic neurotransmission in animals. Most insects studied so far possess two AChE genes: *ace-1* paralogous and *ace-2* orthologous to *Drosophila melanogaster ace*. We characterized the catalytic domain of *Anopheles gambiae* AChE1 in a previous study (Jiang et al., 2009) and report here biochemical properties of *A. gambiae* AChE2 expressed in *Sf*9 cells. An unknown protease in the expression system cleaved the recombinant AChE2 next to Arg^{110}, yielding two non-covalently associated polypeptides. A mixture of the intact and cleaved AChE2 had a specific activity of 72.3 U/mg, much lower than that of *A. gambiae* AChE1 (523 U/mg). The order of V_{max}/K_M values for the model substrates was acetylthiocholine > propionylthiocholine ≈ acetyl-(β-methyl)thiocholine > butyrylthiocholine. The IC_{50}'s for eserine, carbaryl, BW284C51, paraoxon and malaoxon were 1.32, 13.6, 26.8, 192 and 294 nM, respectively. *A. gambiae* AChE2 bound eserine and carbaryl stronger than paraoxon and malaoxon, whereas eserine and malaoxon modified the active site Ser^{232} faster than carbaryl or paraoxon did. Consequently, the k_i's were 1.173, 0.245, 0.029 and 0.018 $\mu M^{-1}min^{-1}$ for eserine, carbaryl, paraoxon and malaoxon, respectively. Quantitative polymerase chain reactions showed a similar pattern of *ace-1* and *ace-2* expression. Their mRNAs were abundant in early embryos, greatly decreased in late embryos, larvae, pupae, and pharate adult, and became abundant again in adults. Both transcripts were higher in head and abdomen than thorax of adults and higher in male than female mosquitos. Transcript levels of *ace-1* were 1.9- to 361.8-fold higher than those of *ace-2*, depending on developmental stages and body parts. Cross-reacting polyclonal antibodies detected AChEs in adult brains, thoracic ganglia, and genital/rectal area. Activity assays, immunoblotting, and tandem mass spectrometric analysis indicated that *A. gambiae* AChE1 is responsible for most of acetylthiocholine hydrolysis in the head extracts. Taken together, these data indicate that *A. gambiae* AChE2 may play a less significant role than AChE1 does in the mosquito nervous system.

Keywords

cholinergic synapse; organophosphate; carbamate; insecticide resistance

Corresponding author: Haobo Jiang, Department of Entomology and Plant Pathology, Oklahoma State University, Stillwater, OK 74078, Tel: (405)-744-9400, Fax: (405)-744-6039, haobo.jiang@okstate.edu.

1. Introduction

Acetylcholinesterases (AChEs) are serine hydrolases mainly associating with the basement membrane around cholinergic nerve terminals of vertebrates and invertebrates, which breakdown acetylcholine to terminate excitatory neurotransmission (Soreq and Seidman, 2001). Due to this critical physiological function and related practical applications, insect AChEs have been purified to various degrees from nerve tissue or expression systems for testing enzyme properties and inhibition by AChE targeting insecticides (Zhu and Zhang, 2005; Walsh et al., 2001; Zhao et al., 2010; Temeyer et al., 2010). Certain mutations in the AChE genes rendered their carriers resistant to insecticides (Oakeshott et al., 2005) and investigations of such resistance led to the discovery of AChE genes and mechanisms of target site insensitivity (Fournier et al., 1989, Weill et al., 2002; Menozzi et al., 2004). We now know most insects have two AChE genes (*ace-1* and *ace-2)* that arose from ancient gene duplication prior to the radiation of Arthropoda (Weill et al., 2002; Kozaki et al., 2008). While a close association of insecticide-resistant AChEs with mutations in *ace-1* suggests its physiological importance (Kono and Tomita, 2006), the role of *ace-2* remains elusive. However, in the lineage of Aristoceran flies, since *ace-1* was lost in the evolution, *ace-2* became indispensable in regulating cholinergic neurotransmission (Hurchard et al., 2006).

Are *ace-1* and *ace-2* both transcribed and translated in nerve tissues of other insects? If so, do they play a similar role by complementing each other? Molecular biological tools have been used to address these questions. For instance, feeding the cotton bollworm *Helicoverpa armigera* with small interfering RNA identical to *ace-2* somehow caused *ace-1* silencing, mortality, growth inhibition, weight loss, and fecundity reduction (Kumar et al., 2009). In the German cockroach *Blattella germanica*, *ace-1* mRNA level was ~10-fold higher than *ace-2*'s in the central nervous system (Kim et al., 2006). Knockdown of *ace-1* expression by RNA interference reduced its protein level and significantly increased the sensitivity to chlorpyrifos, whereas *ace-2* silencing in the cockroach did not affect mortality to the organophosphate (Revuelta et al., 2009). This result agrees with the observation that *B. germanica* AChE1 represents ~70% of the total activity in nerve tissue (Kim et al., 2010). Since, unlike other insects, the cockroach AChE1 has lower catalytic efficiency (V_{max}/K_M: 58.8 $min^{-1}ml^{-1}$) than AChE2 does (234 $min^{-1}ml^{-1}$) (Kim et al., 2010), the AChE1 level has to be much higher in the cockroach tissues to account for the majority of acetylcholine hydrolysis. In another study, silencing *ace-1* in 20-day-old *Tribolium castaneum* increased larval susceptibility to AChE inhibitors and caused 100% mortality within two weeks after eclosion (Lu et al., 2012b). Silencing *T. castaneum ace-2* delayed development and reduced egg laying and hatching. One of the two AChEs detected in the mosquito *Culex pipiens* had much lower sensitivity to malaoxon than the other (Bourguet et al., 1997). So far, thorough comparisons of gene expression and enzyme properties are not available in other insects possessing both *ace-1* and *ace-2*.

The mosquito *Anopheles gambiae* is a major vector of malaria parasites, containing both AChE genes (Weill et al., 2002). We previously expressed and characterized the catalytic domain of AChE1, which has a specific activity much higher than AChEs from other orders of insects (Jiang et al., 2009). It tightly binds eserine, rapidly reacts with a carbamate, and exhibits product inhibition by choline. In this study, we characterized *A. gambiae* AChE2 (38% identical in amino acid sequence to *A. gambiae* AChE1) and compared its biochemical properties with those of the AChE1. We further examined their gene expression patterns by quantitative real-time polymerase chain reaction (qRT-PCR), detected the proteins by immunohistochemistry, and discussed their relative contributions to cholinergic neurotransmission.

2. Materials and Methods

2.1. Chemicals

acetylthiocholine iodide (ATC), acetyl(β-methyl)thiocholine iodide (AβMTC), propionylthiocholine iodide (PTC), *S*-butyrylthiocholine iodide (BTC), 5,5-dithio-bis(2-nitro- benzoic acid) (DTNB), carbaryl, eserine hemisulfate, and 1,5-bis(4-allyldimethyl-ammonium phenyl)-pentan-3-one dibromide (BW284C51) were purchased from Sigma-Aldrich. Paraoxon (O,O′-diethyl *p*-nitrophenyl phosphate) and malaoxon (O,O′-dimethyl S-(1,2-dicarbethoxy)ethyl phosphorothioate) (Chem Service), Clear-Rite 3 (Richard-Allan Scientific), paraformaldehyde, goat-anti-mouse/rabbit IgG-conjugated to alkaline phosphatase (Sigma-Aldrich), nitro-blue tetrazolium (NBT) and 5-bromo-4-chloro-3-indoryl phosphate (BCIP) (Bio-Rad) were purchased from the enlisted vendors.

2.2. Mosquito culture and tissue sectioning

The G3 strain of *A. gambiae* was obtained from Mark Benedict and Malaria Research and Reference Reagent Resource Center (MR4)/American Type Culture Collection (ATCC). The mosquitoes were reared as described by Benedict (1997) with minor modifications. Larvae were reared at 27°C and fed a mixture of baker's yeast and ground fish food (Vitapro Plus Staple Power Flakes, Mike Reed Enterprises). Adults were maintained at 27°C with 85% relative humidity and were fed 10% sucrose. Adult females were fed heparinized equine blood with a membrane feeder (Hemotek). Tissue sections were prepared from 40 adults (day 5). Wings and legs were removed and two gaps were made in the cuticle of each adult with a forceps, one from the thorax and the other from the abdomen, to allow the fixative (0.25% Triton-X100, 4% paraformaldehyde, and 0.1 M sodium phosphate, pH 7.2) to enter. After fixation for 3.5 h at room temperature, the specimens were treated with 70% ethanol overnight, stored at 4°C, and embedded in melted paraffin. Embedding and sectioning were performed in Oklahoma Animal Diseases and Diagnosis Laboratory.

2.3. A. gambiae AChE2 cDNA cloning and sequence analysis

Three cDNA clones (BM632651 from RSP strain; BX621591 and BX619729 from a mixture of PEST, 4arr, M2, Kisumu and RSP strains at different life stages) (Fig. 1) were kindly provided by Dr. Neil Lobo in the Department of Biological Sciences at University of Notre Dame and completely sequenced using the BigDye Terminator Cycle Sequencing Ready Reaction Kit (PE Applied Biosystems). One 5′ fragment (missing in the EST clones) was amplified by semi-nested PCR using *ace2*-specific primers (Table S1, PCR1 and PCR2) and a cDNA pool of adult *A. gambiae* G3, a generous gift from Dr. Susan Paskewitz in the Department of Entomology at University of Wisconsin-Madison. After electrophoresis, the PCR product at expected size was recovered from agarose gel, cloned into pGem-T (Promega), and sequenced. Exon-intron organization of *A. gambiae ace-2* was deduced by comparing the assembled cDNA with its corresponding genomic sequence (GenBank accession number BN000067). Signal peptide and glycosylation sites were predicted using SignalP, NetNGlyc, and NetOGlyc (http://www.cbs.dtu.dk/services/). The 25~30-residue region unique to some insect AChE2s (Weill et al., 2002), catalytic triad, disulfide connectivity, and conserved hydrophobic residues lining the active site gorge were identified through sequence comparison using BLASTP (http://blast.ncbi.nlm.nih.gov/).

2.4. Construction of AChE2/pMFH$_6$ and recombinant baculovirus

Another 5′ AChE2 fragment, not found in the three cDNA clones, was amplified from the adult cDNA pool (Table S1, PCR3 and PCR4), cloned into pGem-T (Promega), confirmed by sequence analysis, and digested with *EcoR*I and *Kpn*I. The 3′ cDNA fragment was amplified using BX621591 as template (Table S1, PCR5) and inserted into pGem-T.

Plasmid DNA was prepared from transformants, confirmed by DNA sequencing, and digested with *Kpn*I completely and *Xho*I partially. DNA fragments at correct sizes (*EcoR*I-*Kpn*I, 1,256 bp; *Kpn*I-*Xho*I, 503 bp; $pMFH_6$ digested with *EcoR*I and *Xho*I, 4,780 bp) were recovered from the gel and ligated. The cloning strategy allows in-frame fusion with the amino-terminal honeybee mellitin signal peptide and the carboxyl-terminal hexahistidine tag, both encoded by the vector (Lu and Jiang, 2008). After transformation, plasmid isolation, and restriction site verification, the recombinant plasmid AChE2/$pMFH_6$ was used to generate a high-titer baculovirus stock (1~2× 10^8 pfu/ml) as described previously (Zhao et al., 2010).

2.5. Expression and purification of A. gambiae AChE2

*Spodoptera frugiperda Sf*9 cells (3.0× 10^6 cells/ml) in 820 ml of Sf-900™ II serum-free medium (Invitrogen Life Technologies) were infected by the viral stock at a multiplicity of infection of 5~10 and grown at 27°C for 80 h with agitation at 100 rpm. After cells were removed by centrifugation at 5000*g* for 10 min, the culture supernatant was diluted with two volumes of buffer A (10 mM sodium phosphate, pH 6.5). Fifty milliliters of dextran sulfate-Sepharose CL-6B beads equilibrated in buffer A was mixed with the supernatant on ice for 1 h. The suspension was loaded to a column (2.5 cm × 20 cm), washed with 200 ml buffer A, and eluted with 200 ml buffer A containing 0.01% Tween-20 and 1.3 M NaCl. Active fractions were pooled, mixed with 10 ml nickel-nitrilotriacetic acid (NTA)-agarose (Qiagen) on ice overnight, and loaded to a column (1.0 cm × 15 cm). After washing with 100 ml phosphate buffered saline (PBS: 2.7 mM KCl, 137 mM NaCl, 10 mM sodium phosphate, pH 7.4) containing 0.01% Tween-20 and 30 mM imidazole, bound proteins were eluted with 30 ml, 300 mM imidazole in the same buffer supplemented with 0.01% Tween-20 and 1.3 M NaCl. The purified AChE2 (0.4 mg) was used as an antigen to raise a rabbit polyclonal antiserum (Cocalico Biological Inc) and the remaining sample was aliquoted and stored at −20°C in the presence of 50% glycerol.

2.6. Determination of protein concentration, enzyme activity, association state, and cleavage site

Protein concentration was determined using Coomassie Plus Protein Assay Kit (Pierce) and bovine serum albumin (BSA) as a standard. AChE activity in 20 μl of 1:5 diluted sample was measured at room temperature by the modified Ellman method (Zhu and Gao, 1999) in a total volume of 100 μl. The final concentrations of ATC and DTNB were 600 and 48 μM, respectively. Absorbance at 405 nm was monitored in the kinetic mode for two minutes on a VERSAmax microplate reader (Molecular Devices). One unit of AChE activity is defined as the amount of enzyme hydrolyzing one μmole of ATC in one minute. Velocity (v) was converted to activity as follows: v (mOD/min) × d (sample dilution factor) ÷ (1.36× 10^4 $M^{-1}{\cdot}cm^{-1}$ × 0.30 cm × 0.02 ml) or 0.0123vd (U/ml fraction). Molecular weight of the native recombinant AChE2 was analyzed on a Zetasizer (Malvern), which measures protein size by light scattering. To estimate cleavage extent, purified AChE2 was separated by SDS-PAGE under reducing condition and visualized by silver staining. After gel scanning and image processing (http://rsbweb.nih.gov/ij/), intensities of all the protein bands were quantified using Digital Science 1D Image Analysis Software (Kodak) to calculate percentage and ratio of the intact and cleaved enzymes in each batch of the purified enzyme. Amino-terminal sequence of a 50 kDa cleavage product was determined at Nevada Proteomics Center (http://www.unr.edu/inbre/Proteomics/). The 16 and 51 kDa cleavage products were in-gel digested with trypsin for mass fingerprint analysis at OSU Recombinant DNA/Protein Resource Facility.

2.7. Kinetics of substrate hydrolysis and enzyme inhibition

Aliquots of the 1:20 diluted enzyme (20 μl, 2.18 μg/ml) were separately reacted with the substrates (80 μl) at final concentrations of 9.375, 18.75, 37.5, 75, and 150 μM. Monitoring of substrate hydrolysis, velocity conversion, and calculation of kinetic parameters (K_M and V_{max}) were carried out as previously described (Zhao et al., 2010). To determine IC_{50}'s, 10 μl aliquots of 1:10 diluted enzyme (4.35 μg/ml) were separately incubated with an equal volume of BW284C51 (2, 10, 20, 50, 100, 200, 1000 nM), carbaryl (2, 10, 20, 50, 100, 150, 200 nM), eserine (0.2, 1, 2, 10, 20, 100, 200 nM), malaoxon (20, 100, 200, 500, 1000, 1500, 2000 nM), or paraoxon (20, 100, 150, 200, 500, 100020, 100, 150, 200, 500, 2000 nM) for 5 min at room temperature. The residual enzyme activity (in reference to a mixture of the enzyme and buffer) was determined by the microplate reader assay and plotted against $-\log_{10}[I]$. IC_{50} for each inhibitor was obtained from nonlinear regression analysis of activity and $\log_{10}[I]$ data using Prism 3.0 (GraphPad Software). Dissociation equilibrium constant (K_d) (*i.e.* affinity constant K_a), unimolecular rate constant (k_2), and bimolecular reaction constant ($k_i = k_2/K_d$) for *A. gambiae* AChE2 inhibition were determined using aliquots of 1:10 diluted enzyme (10 μl, 4.35 ng/μl), 80 μl ATC-DTNB, and 10 μl inhibitor at various concentrations. The experiments were performed with four replicates for each concentration of a compound premixed with the substrate solution. Absorbance monitoring and data analysis were carried out as described by Zhao et al (2010).

2.8. Determination of expression profiles by quantitative real-time PCR (qRT-PCR)

Total RNA samples were prepared from mosquitoes at various developmental stages or from body parts of female and male adults using the Tri reagent method (Sigma-Aldrich) for detecting differential expression of *ace-1* and *ace-2*. Genomic DNA was removed with DNase I (amplification grade, Invitrogen), and DNase I was removed by extraction with phenol and chloroform. First strand cDNA pools were produced from 1.0 μg RNA (developmental profile) or 0.2 μg RNA (body part profile) with QuantiTect Reverse Transcription Kit (Qiagen) and a mixture of oligo(dT) and random primers. After 1:10 dilution, 4.0 μl of cDNA (equivalent to starting with 200 ng total RNA) was used as template for qRT-PCR analysis in duplicate in each 15 μl reaction containing 1× FastStart Universal SYBR Green Master (Rox) (Roche Applied Science) and 333 nM each of specific primers for *ace1*, *ace2*, or *actin* (Table S1, PCR6, PCR7, and PCR8). After PCR was complete on a MyiQ Single-Color RT-PCR Detection System (Bio-Rad), melt curves of the PCR products (158, 154, and 165 bp) in all reactions were examined to ensure proper shape and T_M values. Absence of primer-dimer and correct sizes of the products were confirmed by agarose gel electrophoresis. Amplification efficiencies (E), measured by amplifying a cDNA sample diluted to 10^{-1}, 10^{-2}, 10^{-3}, 10^{-4} and 10^{-5} using specific primer pairs under the same conditions, were 96.7% (*actin*), 88.8% (*ace1*), and 83.5% (*ace2*). Relative *ace* mRNA levels were calculated as: $(1+E_{actin})^{Ct,\ actin}/(1+E_{ace})^{Ct,\ ace}$ (Rieu and Powers, 2009).

2.9. Immunohistochemical detection of AChEs in tissue sections

An immunohistochemical staining protocol (Kim et al. (2006) was adopted to examine distribution of the AChEs in adult tissues. The slides were first treated with Clear-Rite 3 (twice, 5 min each) to remove paraffin. The sections (6 μm thick) were rehydrated by passing through an ethanol series (100, 100, 95, 90, 70, and 50%, 30 s each), incubated with PBST (0.05% Tween-20 in PBS) twice (5 min each), and blocked with 200 μl, 3% BSA in PBST with cover slips on for 1 h in a humidity chamber. The AChE1 or AChE2 antiserum was 1:500 diluted with 3% BSA in PBST and added onto slides (200 μl each). Pre-immune serum (200 μl, 1:500 diluted) was used as a negative control. After 2 h incubation at room temperature, cover slips were removed and slides were washed with PBST (3 times, 10 min each) at room temperature with shaking. Goat-anti-rabbit IgG conjugated to alkaline phosphatase (200 μl, 1:1000 diluted in PBST containing 3% BSA) was added to each slide.

After incubation for 2 h, the slides were washed, and developed in NBT-BCIP substrate solution for 10 to 20 min at room temperature. The slides were examined under a Zeiss Axiophot microscope.

2.10. In-gel assay of AChE activities in mosquito tissue extracts

In order to distinguish the AChEs by gel electrophoresis, activity staining, antibody recognition and mass spectrometry, heads from 4th instar larvae and day 3~5 adults (40 each) of *A. gambiae* were dissected under a microscope and separately homogenized in 400 μl of ice-cold 0.1% Triton X-100 in 0.1 M sodium phosphate, pH 7.4 with a polytron. After centrifugation at 10,000×*g* for 15 min at 4°C, the supernatants were collected for total protein and activity measurement (*Section 2.6*). Same amount of the extracts (7.3 μg protein per lane) were resolved by 10% native PAGE in the Laemmli buffer system. Following electrophoresis, the gel was developed in ATC solution with gentle agitation (Karnovsky and Roots, 1964). After image scanning, the activity band was cut from the gel and digested with trypsin for nonoLC-tandem mass spectrometric analysis at OSU Recombinant DNA/ Protein Resource Facility. The major activity band in a separate lane was cut out, treated with 1×SDS sample buffer, and separated by 7.5% SDS-PAGE under reducing condition. In other lanes of the same gel, the head extracts were directly treated with 1×SDS sample buffer and loaded at 7.3 μg per lane. After electrotransfer, the blot was blocked, incubated with AChE1 or AChE2 primary antibody and then goat-anti-rabbit IgG conjugated to alkaline phosphatase, and developed in NBT-BCIP substrate solution.

3. Results

3.1. Features of A. gambiae AChE2 gene and cDNA

Three EST clones (BX621591, BM632651 and BX619729) contained incomplete open reading frames ranging from nucleotides 1098–1976, 1521–1976 and 1692–1976, respectively (Fig. 1). A 281 bp region (nucleotides 2203–2484, CT…AG), found in BM632651 and BX619729 but not in BX621591, represented a cryptic intron in the 3′ untranslated region. We amplified, cloned, and sequenced a 5′ fragment of *A. gambiae* AChE2 cDNA (nucleotides 1–1137) and assembled it with the EST sequences. The entire coding region (nucleotides 39–1976) encoded a 31-residue signal peptide for secretion and a 614-residue mature protein. Sequence comparison of the cDNA and gene revealed nine exons and eight introns (excluding the cryptic one). Only introns 7 and 8 are located in the same positions and have the same phases as those in *A. gambiae ace-1*, suggesting that these two genes diverged from each other early.

3.2. Structural properties of A. gambiae AChE2

The enzyme lacks a 120-residue, Ser- and Ala- rich region between the signal peptide and catalytic domain, found in many insect AChE1s (Jiang et al., 2009). The catalytic triad of *A. gambiae* AChE2 consists of Ser^{232}, Glu^{361} and His^{475} (equivalent to S^{200}, E^{327} and H^{440} of *Torpedo californica* AChE (pdb 1EA5)). It also contains the hydrophobic residues (W^{83}, W^{141}, M^{148}, Y^{157}, W^{265}, L^{322}, F^{324}, F^{365}, F^{368}, and W^{467}, equivalent to W^{84}, W^{114}, Y^{121}, Y^{130}, W^{233}, F^{288}, F^{290}, F^{331}, Y^{334}, and W^{432} of *T. californica* AChE) lining the active site gorge. The conserved Phe^{292} in *Torpedo* AChE, however, is substituted by hydrophilic Ser^{326} in *A. gambiae* AChE2. The catalytic domain of both enzymes contains six absolutely conserved Cys residues, likely to form three disulfide bonds (Fig. 1). There are two additional Cys residues: Cys^{284} is a buried insect-specific cysteine residue that is prevalent in insect AChE2s (Pang et al., 2012); Cys^{580} may form a disulfide link between two AChE2 subunits, as demonstrated in *Drosophila* AChE (Mutero and Fournier, 1992). The exon 9 encoded a carboxyl-terminal tail (residues 579–614) may be critical for self-association via

the interchain disulfide bond and for membrane anchorage via glycosylphosphatidylinositol (Kakani et al., 2011; Kim et al., 2010; Hass et al., 1988).

3.3. Recombinant production and characterization

To further study the properties of *A. gambiae* AChE2, we amplified the 5′ and 3′ cDNA fragments and cloned them into $pMFH_6$. With the signal peptide and membrane anchoring region replaced by honeybee mellitin secretion peptide and hexahistidine tag respectively, the protein is equivalent to the recombinant *A. gambiae* AChE1 (Jiang et al., 2009), whose amino-terminal extension was removed. After sequence verification, the recombinant plasmid was used to generate a viral stock through transposition, transfection, and serial amplification. Deduced from the cDNA insert, the mature AChE2 has the following sequence: G^{1}IRLV···PCKLDDHTSLEHHHHHH^{594}, in which the underlined portion is identical to residues R^{4} through S^{587} of *A. gambiae* AChE2 (Fig. 1). The calculated M_r and isoelectric point of the recombinant protein are 66896.3 Da and 5.36.

Under the experimental conditions, *A. gambiae* AChE2 was secreted by virus-infected *Sf9* cells at a final concentration of ca. 0.737 μg/ml and 0.061 U/ml. Following an ion exchange step, captured proteins were eluted from the dicationic resin in an enriched form free of medium or nucleic acids with a 4.9-fold increase in specific activity (Table 1). The recombinant protein tightly bound to Ni^{2+}-NTA agarose and, while 30 mM imidazole efficiently removed loosely associated proteins, most AChE2 remained attached to the column until 300 mM imidazole was applied. The eluted enzyme (0.326 mg, ca. 87% pure) had a specific activity of 72.3 U/mg, while the overall purification factor and yield were 246-fold and 50%, respectively.

The purified protein migrated on the SDS polyacrylamide gel mainly as 51 and 16 kDa bands in the presence of dithiothreitol (DTT) and as 130, 100, and 16 kDa bands in the absence of DTT (Fig. 2A), suggesting that the protein formed as a homodimer linked by an interchain disulfide bond as demonstrated in the catalytic domain of *A. gambiae* AChE1 (Jiang et al., 2009). This was consistent with the molecular weight of native protein (162 ± 25 kDa), measured by light scattering. With a theoretical M_r close to 67 kDa, a majority (ca. 81%) of the intact protein appeared to be cut by an unknown protease into two polypeptides. As the 16 kDa band was separated from the 51 kDa band on SDS-PAGE under both conditions, its likely association with the heavy chain was not through a disulfide bridge. Peptide mass fingerprint analysis indicated the 16 kDa light chain is located at the amino terminus whereas the 51 kDa heavy chain represents the carboxyl-terminal fragment of the cleaved protein. Monoclonal antibody against the carboxyl-terminal affinity tag recognized the 51 kDa band (Fig. 2B, upper panel) as well as a 67 kDa one (data not shown), but not the light chain. Polyclonal antibodies against the purified *A. gambiae* AChE2, however, recognized the 16 kDa fragment as well (Fig. 2B, lower panel). Consistent with the prediction of two *N*-linked glycosylation sites (Asn^{88} and Asn^{488}), *N*-glycosidase F treatment increased the mobility of both heavy and light chains. On the other hand, no change was observed after *O*-glycosidase treatment and homologous modeling indicated that Thr^{380} is buried inside the molecule (data not shown). Therefore, the prediction of Thr^{380} as an *O*-glycosylation site (Fig. 1) on the heavy chain may be incorrect. We determined the first five residues of the 51 kDa band as Gly-Leu-Asn-Phe-Gly. By comparing with the sequence of *A. gambiae* AChE2, we identified the proteolytic cleavage site between Arg^{110} and Gly^{111}, which resides in a 28-residue region abundant in charged and other hydrophilic residues (Fig. 1). This region is uniquely found in orthologous AChEs of some dipteran insects (data not shown).

3.4. Substrate specificities

We measured the kinetic parameters of *A. gambiae* AChE2 using a panel of four substrates at various concentrations and found that the enzyme-catalyzed hydrolysis generally followed the Michaelis-Menten kinetics (Fig. 3). As revealed by the K_M values (Table 2), *A. gambiae* AChE2 seemed to bind ATC, BTC or PTC better than AβMTC. Since the hydrolysis of AβMTC, PTC, and ATC was faster than that of BTC, relative catalytic efficiencies of ATC, PTC, and AβMTC, as indicated by the V_{max}/K_M ratios (9.75, 7.11, and 6.06 $L \cdot mg^{-1} \cdot min^{-1}$, respectively), are similar to each other but 2.6- to 4.2-fold higher than that of BTC (2.33 $L \cdot mg^{-1} \cdot min^{-1}$). In other words, acetylcholine (rather than butyrylcholine) may be the natural substrate of *A. gambiae* AChE2.

3.5. Inhibition kinetics

A. gambiae AChE2 was strongly inhibited by eserine, carbaryl and BW284C51, but less so by paraoxon or malaoxon (Fig. 4). The IC_{50}'s of malaoxon (0.294 μM) and paraoxon (0.192 μM) was ca. 22 and 7 times as high as those of carbaryl (13.6 nM) and BW284C51 (26.8 nM), respectively (Table 3). Eserine, another carbamate, blocked 50% of the *A. gambiae* AChE2 activity at an even lower concentration of 1.32 nM. To better understand the susceptibility of *A. gambiae* AChE2 to these inhibitors, we measured kinetic parameters for eserine, carbaryl, paraoxon, and malaoxon (Fig. 5 and Table 4). The affinity constants (K_a's) indicated that the AChE2 bound carbaryl (2.90 ± 0.27 μM) or eserine (3.60 ± 2.81 μM) much tighter than paraxon (34.4 ± 0.7 μM) or malaoxon (97.0 ± 16.0 μM). The Michaelis complex of *A. gambiae* AChE2 and eserine converted to an acyl-enzyme intermediate at a rate (k_2: 3.97 ± 0.97 min^{-1}) higher than that of malaoxon (1.71 ± 0.24 min^{-1}), carbaryl (0.72 ± 0.07 min^{-1}), and paraoxon (0.36 ± 0.01 min^{-1}). Consequently, eserine has the highest k_i (1.17 ± 0.04 $\mu M^{-1} min^{-1}$) and is more potent than the other three inhibitors (k_i: 0.018–0.245 $\mu M^{-1} min^{-1}$). The k_i values of these four compounds are in an order similar to their IC_{50}'s.

3.6. Expression patterns of A. gambiae ace-1 and ace-2

qRT-PCR generated various amounts of products at the expected sizes from cDNAs of mosquitoes at different stages (data not shown). The *ace-1* and *ace-2* mRNA levels were much lower in the larvae, pupae, and pharate adults than in eggs and adults (Fig. 6A). Transcript abundances of *ace-1* were 1.9- to 226.2-fold higher than those of *ace-2* across different developmental stages. Adult males had 2.9- (*ace-1*) and 1.9-fold (*ace-2*) higher mRNA levels than adult females. As the mRNA levels were high in adults, we further examined the transcripts in different parts of adult mosquitoes (Fig. 6B) and confirmed *ace-1* mRNA abundances were 1.9- to 361.8-fold higher than *ace-2*'s. Thorax contained lower mRNA levels of *ace-1* (8.9- and 8.6-fold) and *ace-2* (19.6- and 2.6-fold) than head or abdomen did in females; in males, thorax also contained lower mRNA levels of *ace-1* (34.2- and 81.1-fold) and *ace-2* (4.3- and 22.9-fold) than head or abdomen did, respectively. The results from microarray analyses (http://funcgen.vectorbase.org/ExpressionData/) indicated that *ace-1* and *ace-2* mRNA levels were higher in male than female adults (Koutsos et al., 2007) and lower in larvae than adults (Marinotti et al., 2005).

3.7. Immunolocalization of A. gambiae AChEs

In hope for detecting differential distribution of the two AChEs in adult tissues, we prepared polyclonal antisera against the purified recombinant proteins. Diluted *A. gambiae* AChE1 antiserum strongly reacted with the purified AChE1 (65 kDa) and weakly recognized the AChE2 (67 kDa, intact; 51 and 16 kDa, cleaved) (Fig. 8C and Fig. 2B). On the other hand, *A. gambiae* AChE2 antibodies reacted with the recombinant AChE1 as strong as with the AChE2. Since pre-absorption using purified proteins failed to completely remove the cross-reacting antibodies, we directly used the diluted AChE2 antiserum to localize both enzymes

and detected intense signals in brain, thoracic ganglia, and genital/rectal area of the adults (Fig. 7, D–F). Similar result was acquired using diluted *A. gambiae* AChE1 antiserum (Fig. 7, G–I). Negative controls using the pre-immune serum did not exhibit any signal in these tissues (Fig. 7, AC). Although the antibodies failed to tell the two enzymes apart, the strong signals and their association with the nervous system supported the general role of AChEs in cholinergic neurotransmission.

3.8. Relative AChE levels in head extracts and their identification

In order to distinguish the AChEs and assess their relative contributions to total acetylcholine hydrolysis, we separated protein extracts on a native polyacrylamide gel, detected the enzyme activity in gel, used the AChE antibodies to recognize proteins in the activity band, and analyzed the band of interest by mass spectrometry. We found specific activity of the head extract from adult ("A") mosquitoes was 6.2-fold higher than that of the larval ("L') head extract (Fig. 8A, *left* panel). Consistent with the enzyme assay result, 7.3 μg of total proteins from adult heads, after separation by native PAGE, yielded a single activity band whose intensity was much higher than that from the same amount of the larval sample at the same position (Fig. 8A, *middle* panel). After in-gel ATC hydrolysis, we cut the major activity band, separated proteins in the gel slice by reducing SDS-PAGE, electrotransferred them onto a membrane, and incubated the blot with diluted AChE2 antiserum. The cross-reacting antibodies detected a 100 kDa major band and a smear on top of it (Fig. 8A, *right* panel), but there was no clear signal at 69 or 53 kDa to indicate that intact or nicked AChE2 co-migrated with the major activity band in the 1st dimension. The natural AChE2, containing the carboxyl-terminal extension (see *Section 3.2*), is 2 kDa larger than the recombinant protein (67 kDa). Hence, the AChE2 may have migrated to a different position on the native gel but its activity was below the detection limit of the in-gel activity assay. Trypsin digestion (of the major activity band from a duplicated "A" lane on the same native gel) and tandem mass spectrometry revealed *A. gambiae* AChE1 in that band but no AChE2 was detected. These results together suggested that AChE1 was responsible for most of the ATC hydrolysis.

Did AChE2 exist at a substantial level in the adult or larval head extract and what is the nature of the 100 kDa band? To address these questions, we directly analyzed the two samples by 7.5% SDS-PAGE under reducing condition. After electrotransfer, the protein blot was incubated with the primary (*i.e.* diluted AChE1 or AChE2 antiserum) and secondary antibodies (Fig. 8B). The immunoblot analysis revealed a prominent band at ca. 100 kDa, whose intensity was much stronger in the "A" lanes than in the "L" lanes. Neither AChE1 nor AChE2 antiserum detected considerable amount of *A. gambiae* AChE2 at 69 or 53 kDa position. Since AChE2 antibodies reacted equally well with the same amount of purified AChE1 and AChE2 (Fig. 8C, *right* panel), the failure to detect 69 or 53 kDa band (Fig. 8B, *right* panel) suggested that AChE2 was present in the head extracts at levels below the detection limit. In comparison, the catalytic domain of *A. gambiae* AChE1 had a calculated molecular mass of 62.9 kDa (Jiang et al., 2009) and an apparent mass of 65 kDa (Fig. 8C). The natural enzyme, with an amino-terminal 120-residue extension rich in Ser residues, was probably *O*-glycosylated (Jiang et al., 2009). In other words, posttranslational modifications may be a reason for the further increase in molecular mass from 80 to 100 kDa. The antibody recognition, consistency between enzyme activities and 100 kDa band intensities of "A' and "L", and mass spectrometric identification all support the hypothesis.

4. Discussion

In this study, we expressed *A. gambiae* AChE2 as an active enzyme in the baculovirus-insect cell system. With its putative membrane anchoring region removed from the carboxyl terminus, the AChE2 was secreted to culture medium in a soluble form and purified by ion

exchange and affinity chromatography. *A. gambiae* AChE2 lacks the amino-terminal extension found in many paralogous AChEs (*i.e.* AChE1s) in insects and, thus, is equivalent to the catalytic domain of *A. gambiae* AChE1 reported earlier (Jiang et al., 2009). We found that their catalytic efficiencies (V_{max}/K_M) towards the model compounds are similar, even though substrate binding and reaction rates of the AChEs differ drastically (Table 2). Both K_M and V_{max} of *A. gambiae* AChE1 for ATC hydrolysis are 13-fold higher than those of *A. gambiae* AChE2 and, therefore, their V_{max}/K_M's are the same (Jiang et al., 2009). Similarly, the AChE2 binds AβMTC, PTC, and BTC with affinities ($1/K_M$) 4.3, 5.4, and 10.9 fold higher than the AChE1 does, while the AChE1 hydrolyzes these substrates 6.4, 7.9, and 4.2 fold faster than the AChE2 does. Based on molecular mass (66,896 Da) of the intact protein and V_{max}, the turnover rate (k_{cat}: 55.2 sec^{-1}) of *A. gambiae* AChE2 is much lower than *A. gambiae* AChE1's (651.7 sec^{-1}) (Jiang et al., 2009). This is partly caused by the contaminants (13.1%) in the AChE2 preparation, which are mostly unrelated to AChE2 as suggested by comparing lane "+DTT" (Fig. 2A) and lane "AChE2" (Fig. 8C, *right* panel). However, structural differences seem to be mainly responsible for the differences. Consistent with these experimental data, computational analysis suggests that *T. castaneum* AChE1 is a robust hydrolase whereas *T. castaneum* AChE2 is catalytically inefficient (Lu et al., 2012a).

With the relative maximum velocities ($V_{max, BTC}/V_{max, ATC}$) of AChE1 and AChE2 being 0.11 and 0.34, respectively, both enzymes (especially AChE1) hydrolyze ATC faster than BTC, indicating that acetylcholine could be their natural substrate. Further evidence for them to be esterases of acetylcholine rather than butyrylcholine was obtained from our inhibition analysis. Ethopropazine had a high IC_{50} of 65.9 μM toward the *A. gambiae* AChE1 (Jiang et al., 2009), and we were unable to determine its IC_{50} to the AChE2 due to the solubility limit (data not shown). In other words, ethopropazine, a relatively selective inhibitor of butyrylcholinesterases, is a poor inhibitor of both AChEs.

Decreases in $V_{max, BTC}/V_{max, ATC}$'s may reflect a functional specialization of paralogous AChEs. Phylogenetic analysis suggested that *ace-1* and *ace-2* in insects arose from an ancient gene duplication that occurred prior to the separation of protostomes and deuterostomes (Weill et al., 2002). The relative velocities of *B. germanica* (0.13) and *A. gambiae* (0.09) AChE1s were substantially lower than those of *D. melanogaster* (0.56), *B. germanica* (0.48), and *A. gambiae* (0.34) AChE2s (Gnagey et al., 1987, Jiang et al., 2009; Kim et al., 2010; Table 2), suggesting that the AChE orthologs are less distinctive than the paralogs in terms of ATC and BTC binding and hydrolysis. This agrees with the notion that insect paralogous AChEs (*i.e.* AChE1s) are evolutionarily closer to vertebrate AChEs (Kim et al., 2010), which have the lowest relative maximum velocities (0.005~0.01). Specifically, Phe^{288} (in *T. californica* AChE), conserved in vertebrate AChEs and substituted by Leu in mammalian butyrylcholinesterases, is responsible for the low rate of BTC hydrolysis by the mammalian AChEs (Vellom et al., 1993). By interacting with Phe^{331}, a rigid π-π stacking is formed to limit the acyl binding pocket of vertebrate AChEs to accommodate butyrylcholine. This Phe pair corresponds to Leu^{328}-Phe^{371} in *D. melanogaster* AChE (Harel et al., 2000), Leu^{324}-Phe^{365} in *A. gambiae* AChE2, and Cys^{407}-Phe^{450} in *A. gambiae* AChE1. The flexibility increase accompanying the loss of π-π interaction in insect AChEs may account for the low but substantial activity of BTC hydrolysis.

In addition to substrate specificity, *A. gambiae* AChE1 and AChE2 differ substantially in their susceptibility to various inhibitors (Table 4; Jiang et al., 2009). Carbaryl binds more tightly to AChE2 (K_a: 2.9 μM) than to AChE1 (4.7 μM) but, because carbamation of AChE2 is 2.56 times slower, its k_i is 46% lower (AChE2: 0.245 $\mu M^{-1}min^{-1}$; AChE1: 0.440 $\mu M^{-1}min^{-1}$). In comparison, eserine, malaoxon and paraoxon associate with AChE2 with affinities 13.8-, 16.6- to 34.4-fold lower than with AChE1. Since covalent modification of

the AChEs occurs at similar rates ($k_{2,\ AChE1}/k_{2,\ AChE2}$: 0.76 for eserine, 0.80 for malaoxon, and 2.19 for paraoxon), $k_{i,\ AChE2}$'s for these inhibitors are 10.0-, 13.4-, and 28.6-fold lower than $k_{i,\ AChE1}$'s, respectively. The lower sensitivity of AChE2 to malaoxon is consistent with a similar finding on *C. pipien* AChEs (Bourguet et al., 1997). Despite the fact that the k_i values of carbaryl and eserine for AChE1 are 1.8- and 10.0-fold higher than those for AChE2, their IC_{50}'s are 6.3- and 5.3-fold higher. This discrepancy seems to be related to the lower concentration of AChE1 used for the IC_{50} measurement – because its $V_{max,\ ATC}$ is 12.6-fold higher than the AChE2's, 2.44 ng of the AChE1 (instead of 43.5 ng AChE2) was used to ensure accurate absorbance monitoring. Within each group (AChE1 or AChE2), the order of IC_{50}'s from low to high agree well with the order of k_i values from high to low.

Structural bases for the difference in substrate specificity and inhibitor selectivity are unclear at present. The amino-terminal extension of *A. gambiae* AChE1 could contribute to the binding specificity. Substitutions in upper rim of the active site gorge (*e.g.* Y^{242}, C^{407}, and F^{411} of the AChE1 vs. M^{148}, L^{322}, and S^{326} of the AChE2 vs. Y^{121}, and F^{288}, F^{292} of *T. californica* AChE) may also contribute to the difference, as the entry site of the active site gorge in the AChE2 is larger and more hydrophilic than that of the AChE1 or *Torpedo* AChE1. Bulkier substrates (*e.g.* BTC) or inhibitor (*e.g.* eserine) hence are relatively better tolerated by AChE2 than AChE1. However, the crystal structure of *D. melanogaster* AChE suggests that the active site gorge, covered by aromatic side chains and narrower than *Torpedo* AChE1's, can still accommodate large substrates or inhibitors by adopting different conformations with little movement of main chain atoms (Harel et al., 2000). Consequently, the contribution of substituted residues in the upper rim may be limited and the loss of rigid **π-π** interaction (see above) is a critical factor.

Additionally, the 28-residue insert in *A. gambiae* AChE2 (Fig. 1) seems to play a role in catalytic efficiency. We have purified several batches of the AChE2 at various ratios of intact and cleaved forms and found that the same amount of the cleaved AChE2 hydrolyzed ATC at a rate ~20% higher than the intact one did (data not shown). In *D. melanogaster, Bactrocera oleae* and *Musca domestica*, the orthologous AChEs were partially cleaved at a similar position (Kakani et al., 2012; Harel et al., 2000; Mutero and Fournier, 1992; Haas et al., 1988; Gnagey et al., 1987; Steele and Smallman, 1976). Interestingly, although the insert sequence is hypervariable, the cleavage site sequence (**R**HG**R***GLN) is nearly identical to **R**HG**R**GAN in the fly AChEs. Since RXXR is a recognition site of intracellular processing enzymes (Devi, 1991), *D. melanogaster* and *M. domestica* AChEs are probably cleaved at the same site. Removing the first half of this 33-residue insert (**R**GANGGEHPNGKQADTDHL) and, thus, destroying the signal **R**HG**R** in *Drosophila* AChE indeed led to a processing defect (Mutero and Fournier, 1992).

Relative contributions of the AChE1 and AChE2 in acetylcholine hydrolysis are determined also by their protein levels which are regulated by transcription and translation. We demonstrated that *ace-1* and *ace-2* mRNA levels were relatively high in 0–14 h embryos (Fig. 6A). Although their functions in embryonic development remain unknown, this result seems to be consistent with the detection of AChE activity in *Drosophila* and *Tribolium* embryos (Zador et al., 1994; Lu et al., 2012a). In the 14–40 h embryos, larvae, pupae, and pharate adults, the two mRNA levels dramatically decreased and *ace-2* mRNA was even rarer than *ace-1* mRNA (*Section 3.6*). In male and female adults, both transcripts increased to levels comparable to or higher than those in the early embryos. We also detected higher *ace-1* and *ace-2* mRNA levels in head and abdomen than in thorax from adults of both sexes (Fig. 6B). In most of the samples, *ace-1* transcripts were at least 5-fold more abundant than *ace-2*'s. Consistent with these, we detected AChE1 but not AChE2 in the head extracts and total AChE activity in the adults was much higher than that in the larvae (Fig. 8). While these positive correlations are interesting, we are fully aware of the possibilities that

synthesis and degradation of *A. gambiae* AChE1 and AChE2 can be different and transcript levels often do not correlate with protein levels. For instance, RNA interference of *ace-1* and *ace-2* in the German cockroach specifically depleted the transcripts but the reduction of proteins were less pronounced, suggesting the enzymes were stable and accumulated during development (Revuelta et al., 2009).

Disappointingly, immunolocalization of *A. gambiae* AChEs in tissues was complicated by the antibody cross-reactivity (Fig. 8C) and by low levels of AChE2 in larval and adult heads (Fig. 8B). Consequently, we are not able to demonstrate AChE2's presence at a specific site to suggest function. On the other hand, we are confident about the major role of AChE1 in the nervous system of the adult mosquito (Fig. 7), based on the results of activity assay, immunoblot analysis, and mass identification of tryptic fragments (Fig. 8). The existence of AChE1 in brain and thoracic ganglia is in line with the regulatory function of AChE in the central nervous system. The strong signal detected in the genital/rectal area is interesting (Fig. 7D). Although a possible function of AChEs in reproduction is unclear, silencing of *H. armigera ace-1* led to a fecundity reduction (Kumar et al., 2009). Knocking down *T. castaneum ace-2* affected its development including reproduction (Lu et al., 2012b): dramatic decreases in egg number, egg hatching, and larval weight of the next generation associated only with females injected with double-stranded *ace-2* RNA. Therefore, it is worth exploring these non-classical functions of AChEs in the mosquito and if such functions rely upon acetylcholine hydrolysis.

Supplementary Material

Refer to Web version on PubMed Central for supplementary material.

Acknowledgments

We thank Drs. Jack Dillwith and Deborah Jaworski for critical comments on the manuscript. We are deeply indebted to Dr. Maureen Gorman in Department of Biochemistry at Kansas State University (KSU), who provided mosquito larvae, pupae, and adults for immuno- localization and *in situ* hybridization and commented insightfully on the test results. Zeyu Peng, a graduate student in Dr. Michael Kanost's laboratory in Department of Biochemistry at KSU, provided *A. gambiae* total RNA samples for the expression profiling. We would like to also thank Dr. Susan Paskewitz in Department of Entomology at University of Wisconsin-Madison for the cDNA pool of adult *A. gambiae* G3. Dr. Yoonseong Park in KSU Department of Entomology and Dr. Michael Reiskind and Ali Zarrabi in Department of Entomology and Plant Pathology at Oklahoma State University provided useful assistance in result discussion and mosquito rearing. This work was supported by National Institutes of Health Grant GM58634. This article was approved for publication by the Director of the Oklahoma Agricultural Experiment Station and supported in part under project OKLO2450.

Abbreviations

AChE	acetylcholinesterase
DTT	dithiothreitol
ATC	acetylthiocholine iodide
AβMTC	acetyl-(β-methyl)thiocholine iodide
PTC	propionylthiocholine iodide
BTC	butyrylthiocholine iodide
DTNB	5,5-dithio-bis(2-nitrobenzoic acid)
BW284C51	1,5-bis(4-allyldimethylammoniumphenyl)-pentan-3-one dibromide
NBT	nitro-blue tetrazolium

BCIP	5-bromo-4-chloro-3-indoryl phosphate
BSA	bovine serum albumin
RT-PCR	reverse transcription-polymerase chain reaction
SDS-PAGE	sodium dodecyl sulfate-polyacrylamide gel electrophoresis
EST	expressed sequence tag

References

Benedict, MQ. Care and maintenance of anopheline mosquito colonies. In: Crampton, JM.; Beard, CB.; Louis, C., editors. Molecular Biology of Insect Disease Vectors: A Methods Manual. Chapman & Hall; New York: 1997. p. 3-12.

Bourguet D, Roig A, Toutant JP, Arpagaus M. Analysis of molecular forms and pharmacological properties of acetylcholinesterase in several mosquito species. Neurochem Int. 1997; 31:65–72. [PubMed: 9185166]

Devi L. Consensus sequence for processing of peptide precursors at monobasic sites. FEBS Lett. 1991; 280:189–194. [PubMed: 2013311]

Gnagey AL, Forte M, Rosenberry TL. Isolation and characterization of acetylcholinesterase from *Drosophila*. J Biol Chem. 1987; 262:13290–13298. [PubMed: 3115978]

Fournier D, Karch F, Bride JM, Hall LM, Bergé JB, Spierer P. *Drosophila melanogaster* acetylcholinesterase gene: structure, evolution and mutations. J Mol Biol. 1989; 210:15–22. [PubMed: 2511327]

Hall LM, Spierer P. The Ace locus of *Drosophila melanogaster*: structural gene for acetylcholinesterase with an unusual 5′ leader. EMBO J. 1986; 5:2949–2954. [PubMed: 3024971]

Harel M, Kryger G, Rosenberry TL, Mallender WD, Lewis T, Fletcher RJ, Guss JM, Silman I, Sussman JL. Three-dimensional structures of *Drosophila melanogaster* acetylcholinesterase and of its complexes with two potent inhibitors. Protein Sci. 2000; 9:1063–1072. [PubMed: 10892800]

Hass R, Marshall TL, Rosenberry TL. *Drosophila* acetylcholinesterase: demonstration of a glycoinositol phospholipid anchor and an endogenous proteolytic cleavage. Biochemistry. 1988; 27:6453–6457. [PubMed: 2975507]

Huchard E, Martinez M, Alout H, Douzery EJ, Lutfalla G, Berthomieu A, Berticat C, Raymond M, Weill M. Acetylcholinesterase genes within the Diptera: takeover and loss in true flies. Proc R Soc Lond Ser B: Biol Sci. 2006; 273:2595–2604.

Jiang H, Liu S, Zhao P, Pope C. Recombinant expression and biochemical characterization of the catalytic domain of acetylcholinesterase-1 from the African malaria mosquito, *Anopheles gambiae*. Insect Biochem Mol Biol. 2009; 39:646–653. [PubMed: 19607916]

Kakani EG, Bon S, Massoulié J, Mathiopoulos KD. Altered GPI modification of insect AChE improves tolerance to organophosphate insecticides. Insect Biochem Mol Biol. 2011; 41:150–158. [PubMed: 21112395]

Kakani EG, Trakala M, Drosopoulou E, Mavragani-Tsipidou P, Mathiopoulos KD. Genomic structure, organization and localization of the acetylcholinesterase locus of the olive fruit fly, *Bactrocera oleae*. Bull Entomol Res. 2012; 12:1–12.

Karnovsky MJ, Roots LJ. A “direct-coloring” thiocholine method for cholinesterase. J Histochem Cytochem. 1964; 12:219–221. [PubMed: 14187330]

Kim JI, Jung SC, Koh HY, Lee SH. Molecular, biochemical and histochemical characterization of two acetylcholinesterase cDNAs from the German cockroach, *Blattella germanica*. Insect Mol Biol. 2006; 15:513–522. [PubMed: 16907838]

Kim YH, Choi JY, Je YH, Koh YH, Lee SH. Functional analysis and molecular characterization of two acetylcholinesterases from the German cockroach, *Blattella germanica*. Insect Mol Biol. 2010; 19:765–776. [PubMed: 20738424]

Kono Y, Tomita T. Amino acid substitutions conferring insecticide insensitivity in *ace*-paralogous acetylcholinesterase. Pestic Biochem Physiol. 2006; 85:123–132.

Koutsos AC, Blass C, Meister S, Schmidt S, MacCallum RM, Soares MB, Collins FH, Benes V, Zdobnov E, Kafatos FC, Christophides GK. Life cycle transcriptome of the malaria mosquito *Anopheles gambiae* and comparison with the fruitfly *Drosophila melanogaster*. Proc Natl Acad Sci USA. 2007; 104:11304–11309. [PubMed: 17563388]

Kozaki T, Kimmelblatt BA, Hamm RL, Scott JG. Comparison of two acetylcholinesterase gene cDNAs of the lesser mealworm, *Alphitobius diaperinus*, in insecticide susceptible and resistant strains. Arch Insect Biochem Physiol. 2008; 67:130–138. [PubMed: 18163527]

Kumar M, Gupta GP, Rajam MV. Silencing of acetylcholinesterase gene of *Helicoverpa armigera* by siRNA affects larval growth and its life cycle. J Insect Physiol. 2009; 55:273–278. [PubMed: 19135057]

Lu Y, Pang YP, Park Y, Gao X, Yao J, Zhang X, Zhu KY. Genome organization, phylogenies, expression patterns, and three-dimensional protein models of two acetylcholinesterase genes from the red flour beetle. PLoS One. 2012a; 7:e32288. [PubMed: 22359679]

Lu Y, Park Y, Gao X, Zhang X, Yao J, Pang YP, Jiang H, Zhu KY. Cholinergic and non-cholinergic functions of two acetylcholinesterase genes revealed by gene-silencing in *Tribolium castaneum*. Sci Rep. 2012b; 2:288. [PubMed: 22371826]

Lu Z, Jiang H. Expression of *Manduca sexta* serine proteinase homolog precursors in insect cells and their proteolytic activation. Insect Biochem Mol Biol. 2008; 38:89–98. [PubMed: 18070668]

Marinotti O, Nguyen QK, Calvo E, James AA, Ribeiro JM. Microarray analysis of genes showing variable expression following a blood meal in *Anopheles gambiae*. Insect Mol Biol. 2005; 14:365–373. [PubMed: 16033430]

Menozzi P, Shi MA, Lougarre A, Tang ZH, Fournier D. Mutations of acetylcholinesterase which confer insecticide resistance in *Drosophila melanogaster* populations. BMC Evol Biol. 2004; 4:4. [PubMed: 15018651]

Mutero A, Fournier D. Post-translational modifications of *Drosophila* acetylcholinesterase: *in vitro* mutagenesis and expression in *Xenopus* oocytes. J Biol Chem. 1992; 267:1695–1700. [PubMed: 1730712]

Oakeshott JG, Devonshire AL, Claudianos C, Sutherland TD, Horne I, Campbell PM, Ollis DL, Russell RJ. Comparing the organophosphorus and carbamate resistance mutations in cholin- and carboxyl-esterases. Chem Biol Interact. 2005; 157:269–275. [PubMed: 16289012]

Pang YP. Novel acetylcholinesterase target site for malaria mosquito control. PLoS One. 2006; 1:e58. [PubMed: 17183688]

Pang YP, Brimijoin S, Ragsdale DW, Zhu KY, Suranyi R. Novel and viable acetylcholinesterase target site for developing effective and environmentally safe insecticides. Curr Drug Targets. 2012; 13:471–482. [PubMed: 22280344]

Revuelta L, Piulachs MD, Bellés X, Castañera P, Ortego F, Díaz-Ruíz JR, Hernández-Crespo P, Tenllado F. RNAi of *ace*1 and *ace*2 in *Blattella germanica* reveals their differential contribution to acetylcholinesterase activity and sensitivity to insecticides. Insect Biochem Mol Biol. 2009; 39:913–919. [PubMed: 19900550]

Rieu I, Powers SJ. Real-time quantitative RT-PCR: design, calculations, and statistics. Plant Cell. 2009; 21:1031–1033. [PubMed: 19395682]

Shapira M, Thompson CK, Soreq H, Robinson GE. Changes in neuronal acetylcholinesterase gene expression and division of labor in honey bee colonies. J Mol Neurosci. 2001; 17:1–12. [PubMed: 11665858]

Soreq H, Seidman S. Acetylcholinesterase – new roles for an old actor. Nat Rev Neurosci. 2001; 2:294–302. [PubMed: 11283752]

Steele RW, Smallman BN. Acetylcholinesterase of the house-fly head. Affinity purification and subunit composition. Biochim Biophys Acta. 1976; 445:147–157. [PubMed: 953031]

Temeyer KB, Pruett JH, Olafson PU. Baculovirus expression, biochemical characterization and organophosphate sensitivity of rBmAChE1, rBmAChE2, and rBmAChE3 of *Rhipicephalus (Boophilus) microplus*. Vet Parasitol. 2010; 172:114–121. [PubMed: 20451328]

Vellom DC, Radić Z, Li Y, Pickering NA, Camp S, Taylor P. Amino acid residues controlling acetylcholinesterase and butyrylcholinesterase specificity. Biochemistry. 1993; 32:12–17. [PubMed: 8418833]

Walsh SB, Dolden TA, Moores GD, Kristensen M, Lewis T, Devonshire AL, Williamson MS. Identification and characterization of mutations in housefly (*Musca domestica*) acetylcholinesterase involved in insecticide resistance. Biochem J. 2001; 359:175–181. [PubMed: 11563981]

Weill M, Fort P, Berthomieu A, Dubois MP, Pasteur N, Raymond M. A novel acetylcholinesterase gene in mosquitoes codes for the insecticide target and is non-homologous to the ace gene in *Drosophila*. Proc R Soc Lond Ser B: Biol Sci. 2002; 269:2007–2016.

Zador E, Budai D. Expression of the acetylcholinesterase gene during development of *Drosophila* embryos. Neurobiol (Bp). 1994; 2:301–309.

Zhao P, Zhu KY, Jiang H. Biochemical properties of the catalytic domain of *Schizaphis graminum* acetylcholinesterase-1 produced by baculovirus-infected insect cells. J Biochem Mol Toxicol. 2010; 24:51–59. [PubMed: 20146377]

Zhu KY, Gao JR. Increased activity associated with reduced sensitivity of acetylcholinesterase in organophosphate-resistant greenbug, *Schizaphis graminum* (Homoptera: Aphididae). Pestic Sci. 1999; 55:11–17.

Zhu, KY.; Zhang, ZJ. Insect acetylcholinesterase and its roles in insecticide resistance. In: Liu, TX.; Le, K., editors. Entomological Research: Progress and Prospect. Science Press; Beijing: 2005. p. 226-234.

- Characterization of *A. gambiae* AChE2 using model substrates;
- Proteolysis next to Arg^{110} and its possible role in enzyme regulation;
- Inhibition kinetics of the enzyme and comparison with *A. gambiae* AChE1's;
- Expression profiles of *ace-1* and *ace-2* mRNAs in the mosquito;
- Localization of *A. gambiae* AChEs in adult tissues.

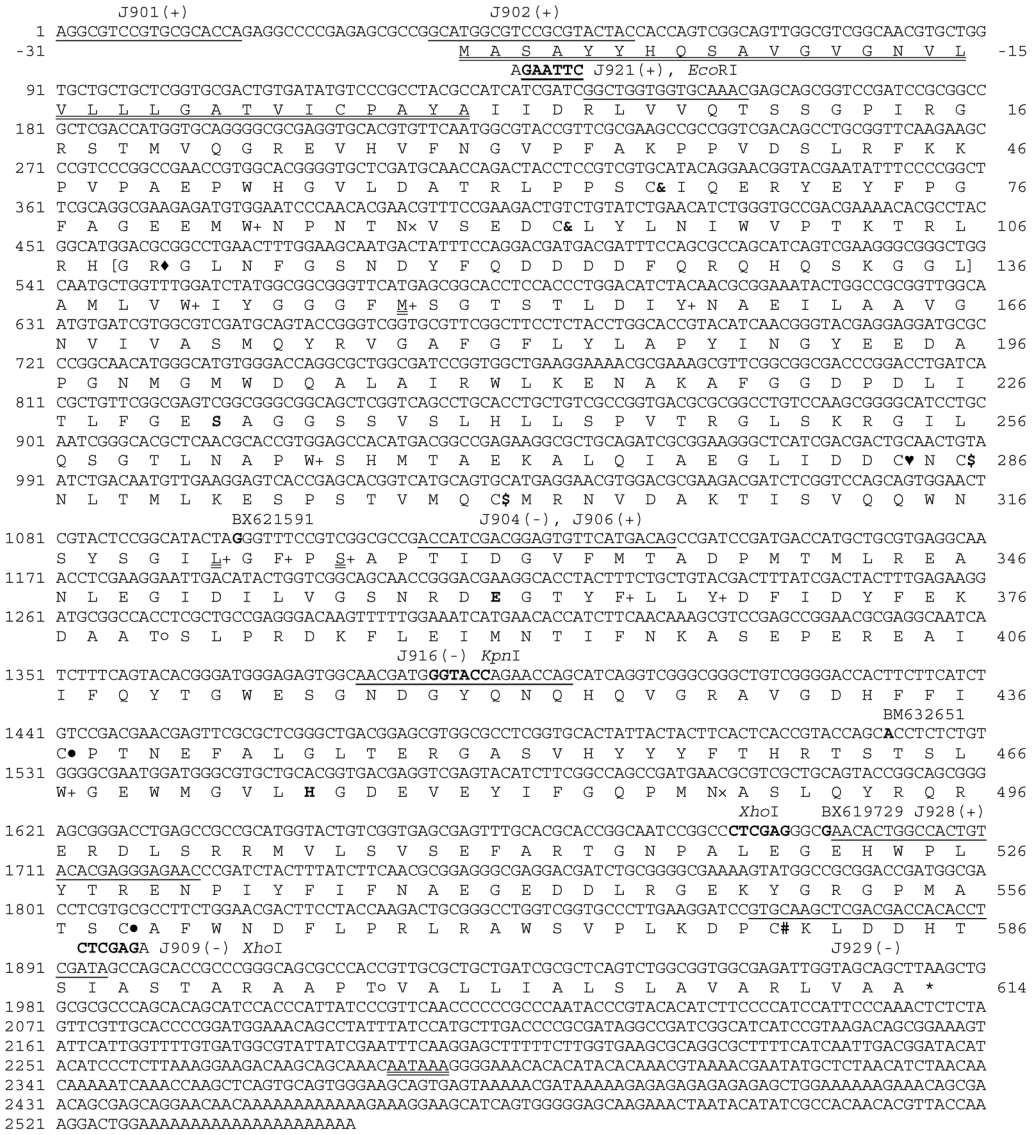

Fig. 1. Nucleotide and deduced amino acid sequences of *A. gambiae* AChE2

The last nucleotide of each exon is *shaded grey* to show the splicing junction. Nucleotides 2203–2484 (CT…AG), missing in cDNA clone BX621591 but retained in clones BM632651 and BX619729, represent a 281 bp cryptic intron of the gene. The starting position of each cDNA is in *bold* and aligned with its clone name. The polyadenylation signal (AATAAA) is *double underlined*. Amino acid residues, shown in one-letter abbreviations, are aligned with the second nucleotide of each codon. The predicted signal peptide (−31 to −1) is *double underlined*, putative *N*-linked (×) and *O*-linked GalNAc (○) glycosylation sites are marked, and the stop codon is indicated by "*". Positions of the Cys residues conserved in all AChEs are marked "& – &, $ – $, and ● – ●" to show disulfide bond connectivity. The unique Cys residue present in many insect AChE1s (Pang, 2006) is replaced by Leu^{322} (*double underlined*). Cys^{284} (♥) is also present in AChEs from *D. melanogaster* (P07140, Hall and Spierer, 1986) and *A. mellifera* (AAG43568, Shapira et al., 2001). Cys^{580} (#) is probably involved in interchain disulfide linkage. The catalytic triad (Ser, His and Glu) is in *bold* and *shaded*, and three of the ten conserved hydrophobic residues (+) lining the active site gorge of many AChEs are replaced by M^{148}, L^{322}, and

Ser^{326} (*double underlined*). The primer binding sites (*underlined*) and names of restriction enzymes used for cDNA cloning and expression in the baculovirus system are indicated. The cleavage site, located in a hydrophilic region (*parenthesized*, residues 109–136) of the protein, is indicated by "◆". The corresponding region (25–30 residues long) is found in some insect AChE2s (Kozaki et al., 2008).

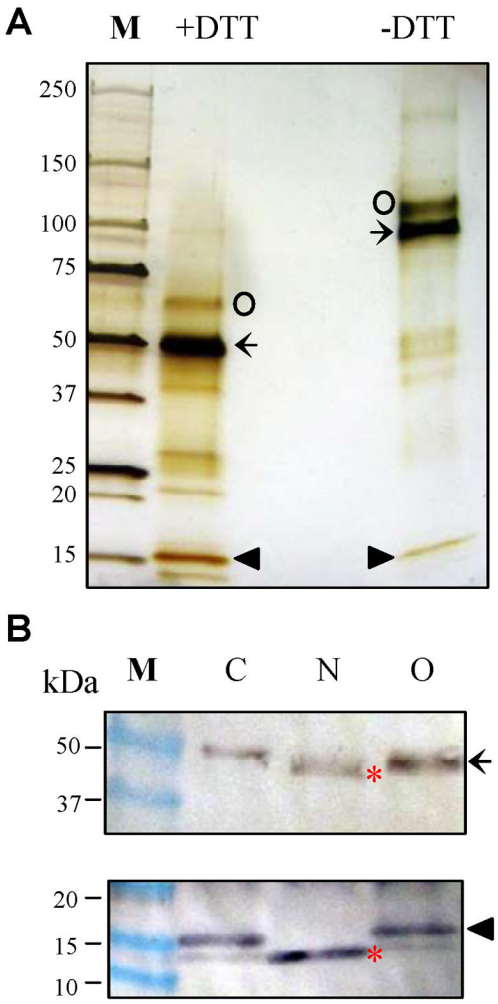

Fig. 2. Association and glycosylation status of the purified *A. gambiae* AChE2 analyzed by SDS-PAGE and immunoblotting

(**A**) The recombinant protein (435 ng) was treated with SDS sample buffer with or without DTT, separated on a precast 4–15% gradient gel, and visualized by silver staining. Intact AChE2 (67 kDa) and its cleavage products (51 and 16 kDa) are labeled by ○, ←, and ▲, respectively. (**B**) The purified enzyme (435 ng) was treated with buffer (lane C), PNGase F (lane N) or *O*-glycosidase (lane O), SDS sample buffer with DTT, separated on the gradient gel, and electrotransferred onto nitrocellulose membrane. Immunblot analysis was performed using diluted anti-$(His)_5$ (*upper* panel) or anti-AChE2 (*lower* panel) serum the primary antibody. Sizes and positions of the M_r markers (lane M) are indicated on the *left*. After deglycosylation with PNGase F, the heavy and light chains (*) migrated faster than the untreated or *O*-glycosidase-treated ones.

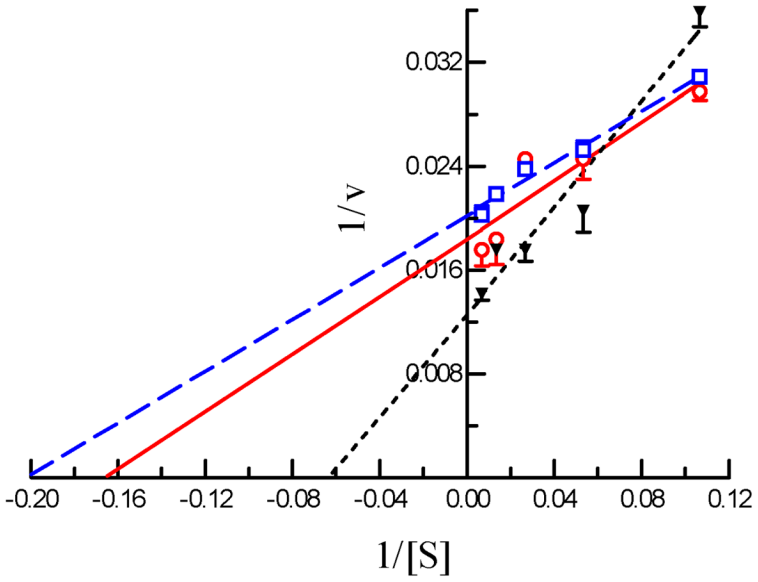

Fig. 3. Enzymatic properties of *A. gambiae* AChE2 determined using model substrates

Hydrolysis of ATC (□- - -□), AβMTC (▼--- ▼), PTC (○—○), and BTC (data not shown) by the purified AChE2 was measured as described in *Section 2.7*. Each point on the double reciprocal plot represents mean ± SEM (n = 4). The r^2 values (or goodness of fit) for ATC, AβMTC, PTC, and BTC are 0.92, 0.90, 0.70, and 0.57, respectively. K_M and V_{max} values for each substrate (Table 2) were derived from v versus [S] plot by the nonlinear regression analysis.

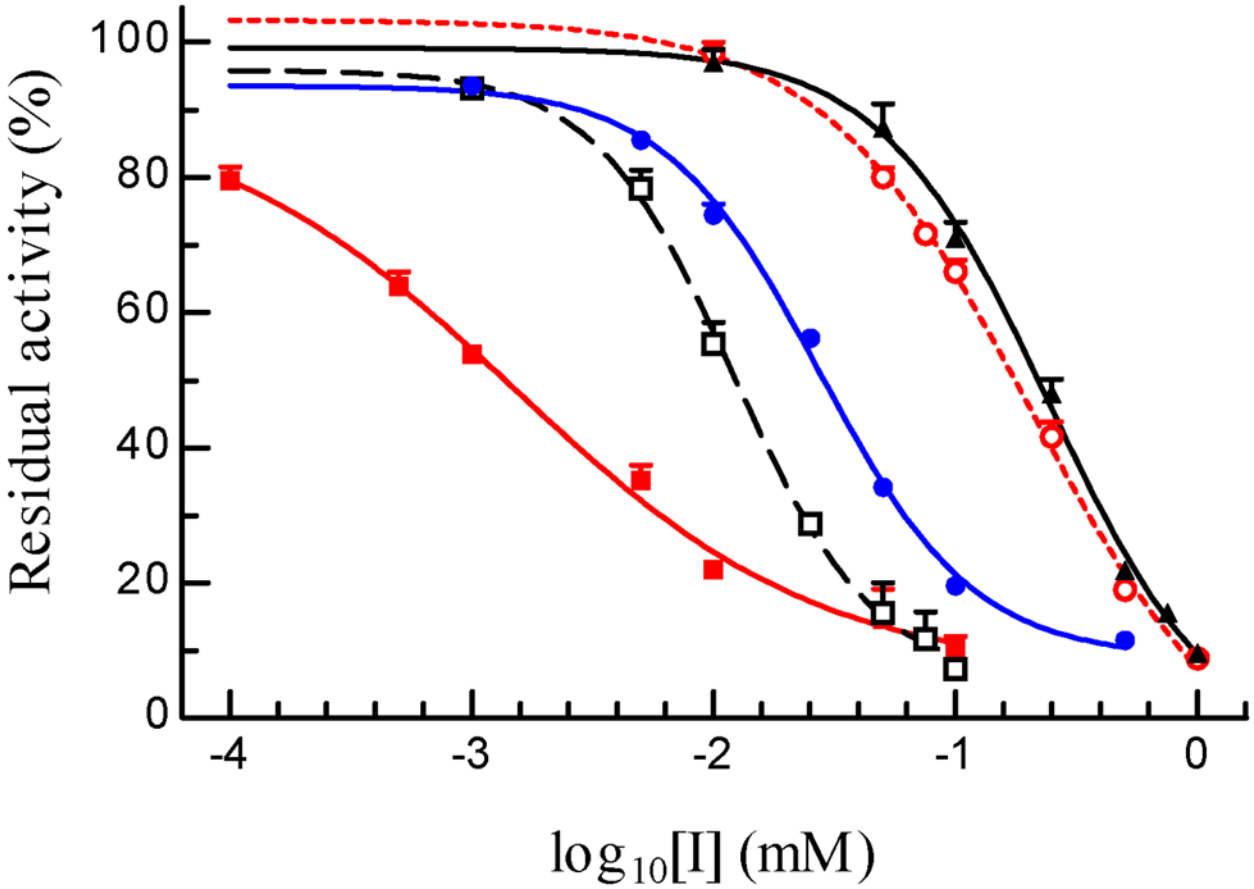

Fig. 4. Inhibition of *A. gambiae* AChE2 by organophosphates, carbamates, and BW284C51 at various concentrations

After aliquots of the purified enzyme (10 μl, 4.35 ng/μl) were separately incubated with 10 μl of buffer, malaoxon (▲ — ▲), paraoxon (○ --- ○), carbaryl (□ – – □), eserine (■ — ■), and BW284C51 (● — ●) at 25°C for 10 min, the mixtures were reacted with ATC-DTNB solution and absorbance changes were monitored by a microplate reader at 405 nm. Residual activities (% of the control of AChE2 and buffer, shown as mean ± SEM (n = 4), are plotted against inhibitor concentrations for IC_{50} calculation (*Section 2.7*).

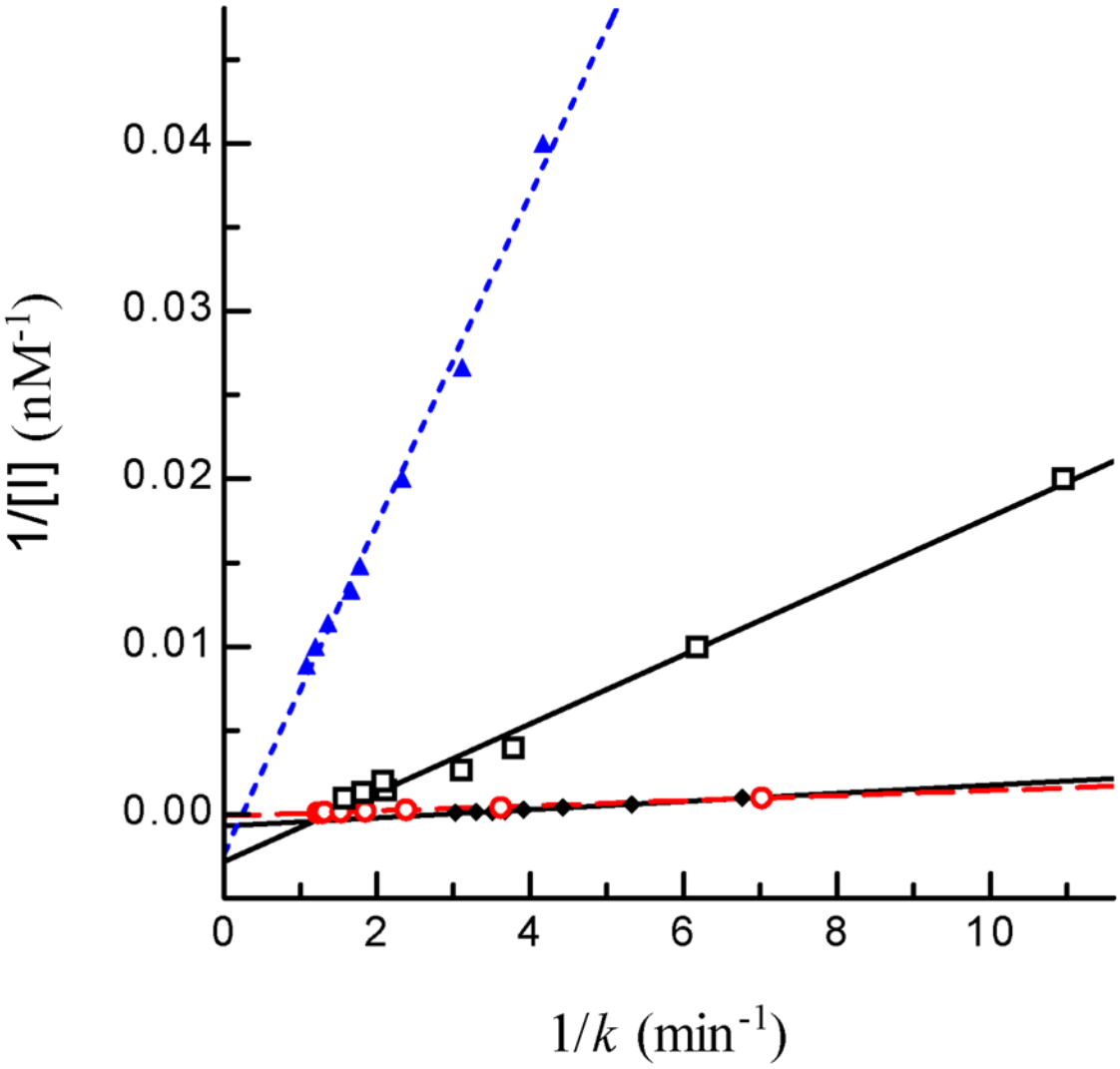

Fig. 5. Determination of K_d and k_2 values of four inhibitors of *A. gambiae* AChE2

Aliquots of the diluted enzyme (10 μl, 4.35 ng/μl) were individually added to 80 μl ATC-DTNB premixed with 10 μl carbaryl (□ —— □), eserine (▲ --- ▲), malaoxon (○ - - ○), or paraoxon (◆ —— ◆) at different concentrations. Absorbance at 405 nm was monitored immediately on the microplate reader at fifteen-second intervals for 5 min and the readings were used to derive *k*'s by curve fitting [$A = A_\infty (1-e^{-kt})$]. Then, $1/k$ and 1/[I] values were plotted and analyzed by linear regression as described in *Section 2.7* ([S] = 600 μM, K_M = 5.075 μM, α = 0.992).

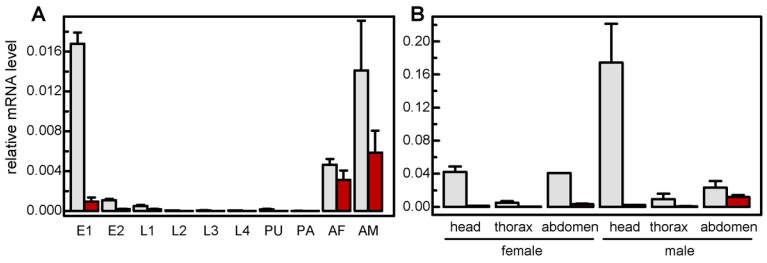

Fig. 6. Transcript levels of *A. gambiae* AChE1 (light bar) and AChE2 (dark bar) at different developmental stages (A) and in three body parts (B)

Total RNA samples were isolated from <14 h (E1) and 14–40 h (E2) eggs, 1st instar (L1), 2nd instar (L2), 3rd instar (L3), and 4th instar (L4) larvae, pupae (PU), pharate adults (PA), day 4 adult females (AF) and males (AM), heads, thorax, and abdomens of adult females and males. The *ace-1* and *ace-2* mRNA levels were analyzed by qRT-PCR as described in *Section 2.8*. Normalization of cDNA templates was performed by using actin as an internal standard according to $(1+E_{actin})^{Ct,\ actin}/(1+E_{ace})^{Ct,\ ace}$. Note that the *ace* transcript levels were much lower than the *actin* control (set at 1.00 for all samples).

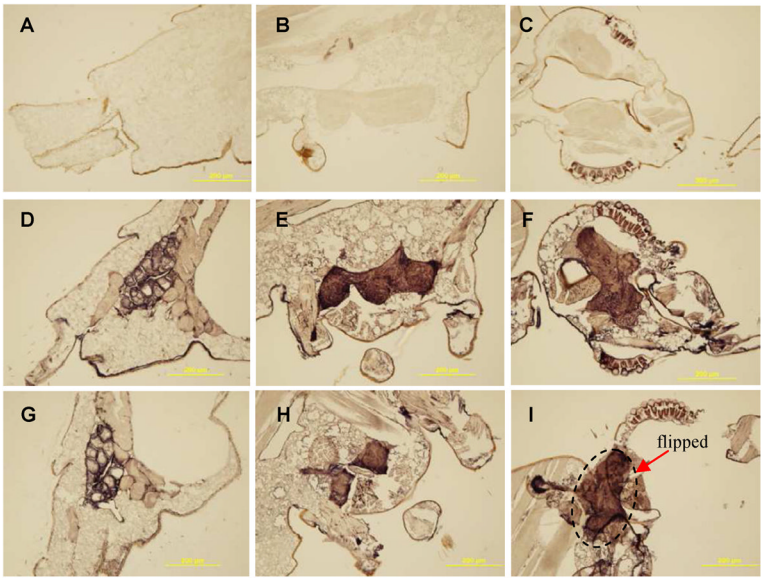

Fig. 7. Immunohistochemical detection of *A. gambiae* AChEs in various tissues

A, D and G, adult terminalis; B, E and H, adult thorax; C, F and I, adult head. Panels A–C: preimmune serum; panels D–F: AChE2 polyclonal antiserum; panels G–I: AChE1 polyclonal antiserum. Note that a piece of brain tissue was flipped onto the neck area during development.

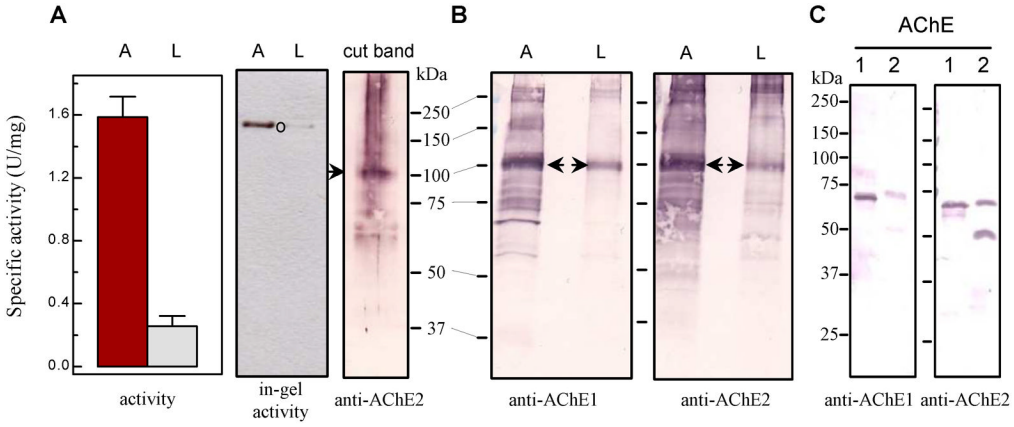

Fig. 8. Separation of proteins in larval and adult head extracts by native PAGE, in-gel activity assay, and immunoblot analysis

(**A**) *Left* panel: Activity assay was performed using adult (A) and larval (L) head extracts (3.25 μg total protein in 20 μl buffer) mixed with 80 μl ATC-DTNB substrate solution (*Section 2.6*); *Middle* panel: in-gel AChE activity staining; *Right* panel (cut band): activity band (marked by ○) was cut from the "A" lane and subjected to reducing SDS-PAGE and immunoblot analysis using diluted AChE2 antiserum as the primary antibody. (**B**) Adult and larval head extracts (7.3 μg protein per lane) were separated by 7.5% SDS-PAGE, transferred onto nitrocellulose membrane, and incubated with diluted AChE1 (*left* panel) and AChE2 (*right* panel). The 100 kDa band (marked by *arrow*) was identified by mass spectrometric analysis as *A. gambiae* AChE1. Sizes and positions of M_r markers are indicated. (**C**) Cross-reactivity of the AChE1 and AChE2 antisera: Purified catalytic domains of *A. gambiae* AChE1 (lane 1, 50 ng) and AChE2 (lane 2, 50 ng) were separated by SDS-PAGE under reducing condition and electrotransferred to nitrocellulose membrane for immunoblot analysis using the diluted AChE1 (*left* panel) or AChE2 (*right* panel) antiserum as the primary antibody.

Table 1

Purification of *A. gambiae* AChE2

sample	volume (ml)	protein		activity		yield (%)	specific activity (U/mg)	purification (fold)
		(μg/ml)	(mg)	(U/ml)	(U)			
medium dextran	800	208.1	166.5	0.0613	49.0	100	0.294	1.00
sulfate	100	302.5	30.25	0.437	43.7	89.2	1.44	4.90
Ni-NTA	7.5	43.5	0.326	3.14	23.6	50	72.3*	246

* The specific activity of pure *A. gambiae* AChE2 is estimated to be 83.2 U/mg, considering 13.1% of total proteins were contaminants in this enzyme preparation. The purity is determined by densitometric analysis, as described in *Section 2.6*. From the enzyme activity (0.0613 U/ml), its concentration in the conditioned medium is calculated to be 0.737 μg/ml. Based on the data of band intensities, the ratio of intact and cleaved *A. gambiae* AChE2 in this enzyme preparation was estimated to be 1:4.2.

Table 2

Kinetic parameters of recombinant *A. gambiae* AChE2 *

substrate	K_M (μM)	V_{max} (U/mg)	V_{max}/K_M (L·mg^{-1}·min^{-1})	k_{cat} (sec^{-1})
ATC	5.08 ± 0.51	49.53 ± 0.81	9.75	55.2 ± 0.9
AβMTC	12.10±2.07	73.35 ± 3.14	6.06	81.8 ± 3.5
PTC	8.21 ± 1.93	58.41 ± 2.96	7.11	65.1 ± 3.3
BTC	7.18 ± 1.54	16.70 ± 0.72	2.33	18.6 ± 0.8

* Results are presented as the mean ± SD (n = 4). Correlation coefficients (r^2) for the four substrates are 0.91–0.99 on the plot of substrate concentration and velocity. Turnover rates (k_{cat}) are calculated based on molecular mass (66,896 Da) of the intact protein and maximum velocity (V_{max}).

Table 3

IC_{50} of inhibitory compounds towards *A. gambiae* AChE2 *

compounds	IC_{50} (M)	95% confidence intervals of IC_{50} (M)	r^2
eserine	1.32×10^{-9}	$0.75 \sim 2.32 \times 10^{-9}$	0.92
carbaryl	1.36×10^{-8}	$0.96 \sim 1.92 \times 10^{-8}$	0.97
BW284C51	2.68×10^{-8}	$2.23 \sim 3.23 \times 10^{-8}$	0.99
paraoxon	1.92×10^{-7}	$1.57 \sim 2.35 \times 10^{-7}$	0.99
malaoxon	2.94×10^{-7}	$2.25 \sim 3.86 \times 10^{-7}$	0.99

* Residual enzyme activity was measured with four repeats for each compound at each concentration as described in *Section 2.7.* The activity and $\log_{10}$[I] data were fitted with the sigmoidal dose-dependent curve (constant slope) using Prism 3.0.

Table 4

Constants for inhibition of *A. gambiae* AChE2 by carbamates and organophosphates*

compounds	K_a (μM)	k_2 (min^{-1})	k_i ($\mu M^{-1}min^{-1}$)
eserine	3.60 ± 2.81	3.97 ± 0.97	1.173 ± 0.043
carbaryl	2.90 ± 0.27	0.72 ± 0.07	0.245 ± 0.093
paraoxon	34.4 ± 0.7	0.36 ± 0.01	0.029 ± 0.011
malaoxon	97.0 ± 16.0	1.71 ± 0.24	0.018 ± 0.007

*Correlation coefficients (r^2) of the linear regressions (p-value < 0.0001) are greater than 0.99.